Assessment of the hydration/dehydration behaviour of MgSO4·7H2O filled cellular foams for sorption storage applications through morphological and thermo-gravimetric analyses

Abstract

In this article, the relationship between morphological characteristics and de/hydration performance was assessed on an innovative magnesium sulphate heptahydrate filled silicone composite foam for sorption thermal energy storage applications. Hydration and dehydration aspects of the foam were investigated by varying salt hydrate filler content. The composite foam showed a mixed open/closed cellular structure, whose morphology was dependent on the filler content present in the formulation. Low salt content foams (40 wt.% and 50 wt.% salt content) highlighted a predominantly open cell structure with a strong interconnection between bubbles. High salt content foams (60 wt.% and 70 wt.% salt content) showed a structure for which the cellular interconnections were more limited.

Compared to pure salt, it was evidenced that salt filled composite foams have a significant de/hydration capacity. The water/salt reaction is not hindered by the foaming process. Based on morphological and thermo-physical properties of the foam a simplified vapour diffusion flow process in composite foams was proposed.

Introduction

Energy production is the fulcrum of economical, scientific and social development worldwide. To achieve energy sustainability different technologies, such as: energy conversion from renewable, use of natural resources (e.g. biomass, wind, solar and water) and energy storage systems for long-term or remote usage are the main promising alternatives to promote the desertion of fossil fuels [1].

The development of advanced Thermal Energy Storage (TES) systems is considered as a crucial topic in order to further support the increase of share of renewable at the building scale [2] as well as to enhance the energy efficiency of industries [3]. TES technology can be classified in three main categories: sensible, latent and thermochemical [4]. In the sensible technology, thermal energy is stored by increasing the temperature of the storage medium, exploiting its heat capacity. In the latent technology, the thermal energy is mainly stored as latent heat of phase transition, usually between solid and liquid state. In the thermochemical technology, thermal energy is stored by a reversible physical or chemical reaction between two components. While sensible and latent TES are quite established technologies, especially from the material point of view [5], the interest in the development of innovative materials for thermochemical storage is increasing [6–8]. Indeed, thermochemical TES represents an attractive solution from different points of view. First, these materials are characterised by energy storage density even one order of magnitude higher than other technologies [9]. Moreover, thermochemical TES allows the efficient implementation of the seasonal storage concept, since the thermal energy is stored as reaction potential between two components. Accordingly, the energy is kept almost indefinitely stored as long as the two components are separated. This avoids the degradation of the energy stored during time due to heat losses towards the environment [10,11].

Within the wide group of thermochemical TES, the sorption TES technology is considered promising, especially for low to medium temperature heat sources (i.e. 80-150°C). Indeed, in this case the interaction between the two components, defined as sorbent and sorbate, involves either physical or chemical reactions, characterised by weak bonding energy, making the charging phase effective already in this temperature range [12]. Usually the sorbate is represented by water vapour, thanks to its high latent heat of evaporation as well as its eco-compatibility and low corrosiveness. Anyway, several studies are still evaluating other possible fluid/sorbent working pairs in order to improve the storage performance of the systems [13]. Within the class of solid sorbents, the classification can be made taking into account the nature of the interaction between the sorbate and the sorbent. Indeed, the salt hydrates are characterised by a chemisorption process due to the hydration/dehydration process of the salt itself [14]. Differently, the adsorbent materials interact with the sorbate by means of physical bonds (e.g. Van der Waals). Different adsorbent materials

were proposed and investigated in the literature, namely, zeolites [15], silico-alumino-phosphates and silica gels [16] and several metal-organics frameworks (MOF) [17]. Both chemisorption and physisorption technologies present some known limitations. Indeed, pure salt hydrates face swelling, agglomeration and corrosion issues during hydration/dehydration process, while, adsorbent materials suffer of poor heat transfer efficiency and limited sorption storage density, due to the lower sorption enthalpy associated to the physisorption process [9]. In order to overcome these issues, sorbent composites were proposed in the literature [18]. This innovative class of materials employs salt hydrates embedded inside a porous structure. In this way, most of the issues related to the employment of pure salt can be overcome, since the porous matrix supports and disperses the salt, increasing heat and mass transfer properties and limiting risk for agglomeration and swelling. Several different sorbent composites were proposed in the literature, varying both porous matrix and salt hydrate [19]. Among them, the most common matrices are silica gel [20], clays [21] and carbonaceous structures [21], while among the salt hydrates LiCl [22], $MgSO_4$ [23] and $SrBr_2$ [21], and $CaCl_2$ [24–26] were deeply investigated. The experimental results reported in the literature confirmed that these materials can achieve promising TES capacities, for instance, the composite LiCl/Vermiculite developed by Grekova et al. [22] can reach up to 2.3 kJ/g under seasonal storage operating conditions. Nevertheless, some critical aspects of the composite sorbent technology needs to be investigated, such as the cycling and the mechanical stability, which can affect the reliability in operation.

In such a context, recently, an innovative concept was proposed by Palomba et al. [27], employing a polymeric macro-porous foam to host $MgSO_4$. The flexibility characteristics of this foam can improve the cycling and mechanical stability of the composite, allowing for an expansion of the salt hydrate volume during the hydration process. Furthermore, the employed matrix is permeable to water vapour, which guarantees a proper hydration/dehydration reaction of the hosted salt. The preliminary thermo-physical and structural characterisations confirmed the reliability of the proposed solution. In the present work, a detailed morphological analysis of different composite sorbents, prepared with variable amount of embedded salt hydrate, was performed, aiming at the evaluation of the effect of the presence of the salt on the foaming process. Particularly, the pore size and shape distribution were correlated to the synthesis conditions and material compositions. Furthermore, the morphological analysis coupled to the results of the measured dehydration performance under real boundary conditions in a thermo-gravimetric apparatus, allowed to define a simplified model of the water vapour diffusion inside the realised composites.

Experimental Part

Foam synthesis

The concept to embed an active filler in siloxane based foam was recently proposed for adsorption heat pump applications, where the silicone porous matrix was used to hold zeolite filler in order to obtain a composite materials with high porosity and good adsorption/desorption capacity [28,29].

Based on this approach, a mixture of poly(methylhydrosiloxane) $(CH_3(H)SiO)_n$ (PMHS) and a silanol terminated polydimethylsiloxane (PDMS) compounds (supplied by Gelest Inc., Morrisville, USA) with proper catalyst was employed to form a silicone foam that represents the hosting matrix for a salt hydrate ($MgSO_4 \cdot 7H_2O$) characterized by excellent adsorption capacity.

The selected polymers were chosen as matrix in the composite foam thanks to their high permeability to water vapour, thus not affecting the water vapour diffusion and therefore the hydration and dehydration stages during the real operating conditions. In *Figure 1*~~figure 1~~ a scheme of the salt-silicone foam samples preparation is reported.

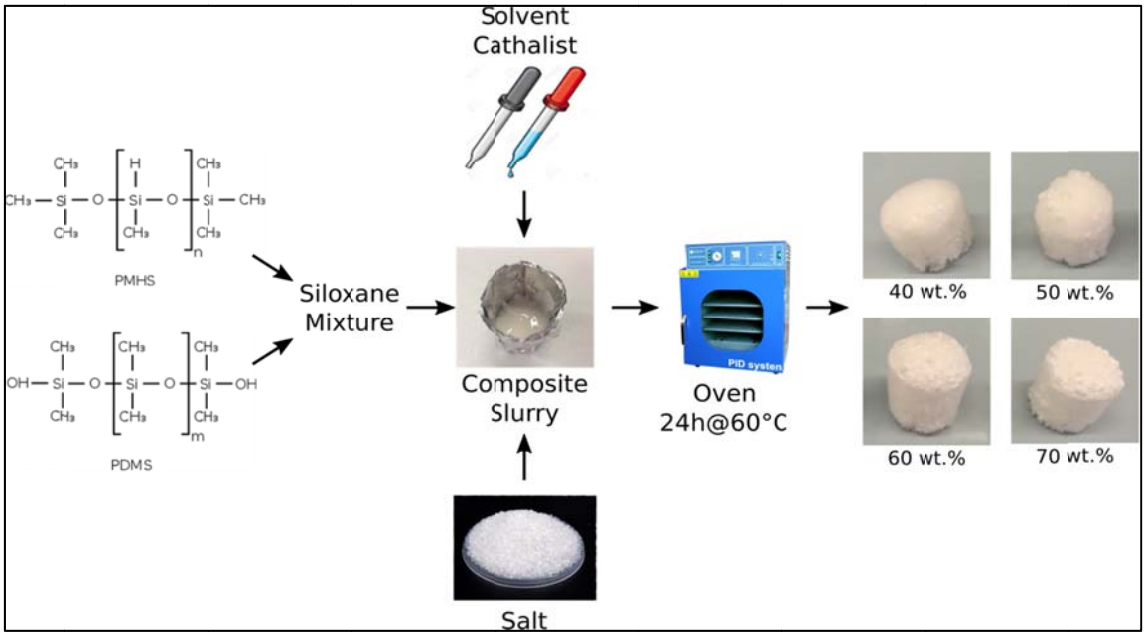

Figure 1: Scheme of the preparation phases of the salt-silicone foams

During the composite compounds mixing, the $MgSO_4 \cdot 7H_2O$ salt was dispersed in different percentages (ranging from 40-70 wt.%) up to reach an homogeneous slurry, and then the foaming process was performed under controlled temperature (60°C for 24h). The detailed synthesis process to obtain the foam is described in [30].

As reference, an unfilled silicone foam was prepared (Mg_0 foam). The reaction, promoted by the addition of the catalyst ((Sn(II) compound) occurring during the synthesis according to [29]:

$$\equiv Si - OH + H - Si \equiv \xrightarrow{Sn(II)} \equiv Si - O - Si \equiv + H_2 \uparrow \quad (1)$$

The reaction between the hydroxyl and hydride groups of PDMS and PMHS, respectively, creates new siloxane Si-O-Si linkages that led to a rubber-like silicone network. Due to the cross-linking reaction, gaseous hydrogen volatile product is formed acting as foaming agent.

The composite foams were identified in the paper with the code "Mg_" followed by a number indicating the salt percentage added to the silicone matrix; e.g. the code "Mg_50" is referred to a foam constituted by 50% of salt hydrate filler. Analogously the code "Mg_0" is referred to foam constituted by pure polymer matrix, without salt hydrate addition.

Foam morphology and surface characterization were evaluated by scanning electron microscope (SEM instrument Philips XL-30-FEG) and 3D optical digital microscope (Hirox HK-8700).

The analysis of the dehydration reaction was performed by means of a modified Labsys Evo Setaram thermo-gravimetric apparatus, whose main features are reported in the literature [31]. The testing protocol was as follows: the sample was weighted in an external microbalance, loaded inside the TG chamber and evacuated at room temperature down to 1 10^{-3} mbar. Then, water vapour produced by an external evaporator was admitted inside the TG chamber. The evaporator was kept at 20°C, in order to obtain a saturated water vapour atmosphere at 23.4 mbar. Finally, the dehydration process was performed by heating up the sample from 30°C to 150°C with a heating rate of 5°C/min, to evaluate the water vapour released. The tests were repeated on different samples to get an evaluation of the measurement uncertainty.

Bubble size distribution

The followed method consisted in performing bubble measurements on contiguous and slightly overlapped images (by using a tiling image reconstruction supplied by Hirox HK-8700) software) of the whole cross section foamed sample. All images were performed at 50x magnification. This approach was used to maximizing statistical information concerning population data [32]. Due to a low contrast between bubbles and composite framework, it was not possible to perform an automatic evaluation of bubble area. Image processing was instead carried out semi-automatically. The perimeter of each bubble was manually traced in the tailed image by using a photo-editor program (Gimp 2.8). Afterwards, the so obtained border regions of bubbles were analysed, by means of an image analysis software (ImageJ 1.48, WS Rasband, ImageJ, US National Institutes of Health) for each foam obtained with different salt percentage. The bubble size population data were clustered into classes according to Sturges rule [33], where the number and the intervals of the classes (Nc and w, respectively) were related by the equations:

$$Nc = 3.322 \log N_b + 1 \quad (2)$$

$$w = \frac{d_{max} \quad d_{min}}{N_c} \tag{3}$$

Where N_b is the number of observed bubbles, d_{min} and d_{max} are smallest and largest measured bubble diameters, respectively. Statistical evaluation was evaluated on the frequency distributions.

Results and Discussion

Foam Morphology: optical observation

In *Figure* ***2*** the stereo-microscope of cross section along the foaming direction of a reference Mg_40 sample is reported.

Visually analysing location, distribution and size of the bubble particles, some heterogeneities on the Mg_40 foam structure can be detected. At the sample sidewalls and base, some voids or elliptical bubbles can be identified.

During the foaming stage, the hydrogen bubbles, generated as a reaction product between the siloxane constituents (PDMS and PMHS), evolve upward. In the bottom of the specimen, a bubble coalescence phenomenon was found. Bubble cells are generally slightly larger than the top side of the foam. However, no preferential foaming direction on the bubbles location can be observed, indicating a good homogeneity of the foaming stage that uniformly occurred. However, it is worth noting some large bubbles, about 3-4 mm in size, mainly with elliptical shape on the sample edges.

In any case, the foam, although characterized by these local defects, is structurally tough and homogeneous. Furthermore, the cell walls are thick enough to guarantee a suitable and reliable mechanical stability. Visually there are no lumps of hydrated salt, which is therefore homogeneously dispersed and integrated into the cellular foam structure.

Figure 2: Stereo-microscope image of interconnected cellular foam structure in Mg_40

By analysing a detail of the sample cross-section, the foam morphology can be better detected. The cellular structure is well defined and interconnected. The bubbles, created during the foaming

phase, are connected by secondary channels to each others, ensuring a very wide continuity channels network. These preferential paths between the bubbles could play a fundamental role in the water vapour flow during the salt hydration/dehydration phase, making this material, potentially, a more effective system for sorption thermal energy storage application.

Figure 3: Stereo-microscope image of cross-section along foaming direction of Mg_70

At increasing salt hydrate content, the coalescence phenomenon is hindered. In *Figure 3*~~figure 4~~ stereo-microscope optical image of cross-section along the foaming direction of Mg_70 foam sample is shown. No preferential bubble flow can be identified. Moreover, conversely of Mg_40 foam, heterogeneity in the peripheral areas of the foam (near the edge) is not identifiable. However, a discontinuity between the upper and lower sides of the foam can be highlighted by analysing the bubble size. In particular, relatively larger bubbles are found in the lower part than the upper one of the specimen. Furthermore, some agglomeration phenomena of the salt hydrate filler occurred. Indeed, some colonies of clusters of salt hydrate crystals are found embedded in the cellular structure of the foam.

A high salt hydrate content within the formulation results in a very high viscosity value of the filler-siloxane composite slurry. This significantly reduces the flow of hydrogen bubbles and their subsequent coalescence during the foaming phase. Consequently, small size bubbles were obtained.

Furthermore, the reduced content of siloxane matrix (30 wt.%) strongly limits the cohesive strength of the foam, though, from a mechanical point of view, no local detachments or loss of foam portions were observed. This aspect indicates that a suitable interaction between siloxane matrix and salt hydrated filler still occurred.

Foam Morphology: Statistical analysis

In order to better study the influence of the addition of salt hydrate on the morphological characteristics of the silicone based foams, a statistical analysis, was carried out on the composite foams with different salt hydrate content, by using digital image analysis of the bubbles distribution. Some relevant statistical parameters at varying filler content are reported in the Table 1.

Table 1: Main statistical parameters on bubble size distribution of salt hydrate composite foams

	Mg_0	***Mg_40***	***Mg_50***	***Mg_60***	***Mg_70***
Salt hydrate [wt.%]	**0.0**	**40.0**	**50.0**	**60.0**	**70.0**
Diameter [mm]	**2.12**	**1.70**	**1.26**	**1.04**	**0.65**
Standard Deviation	**3.22**	**3.14**	**2.95**	**1.99**	**1.28**
Coefficient of Variance	**1.52**	**1.84**	**2.34**	**1.91**	**1.95**
Circularity	**0.62**	**0.53**	**0.57**	**0.59**	**0.60**

Standard deviation (SD) was used to quantify the data dispersion around the average value. A low SD value indicates that the data points tend to be close to the average value of the set, while a high SD indicates a wide data dispersion. However, when datasets are characterised by different mean values, the SD is not sufficient to make a comparison among the data. Consequently, also the coefficient of variance (CoV) was calculated, as statistical parameter to evaluate the variability of data dispersion. Indeed, it is defined as the ratio between the SD and the mean value. Accordingly, it is independent on the unit in which the measurement was performed, being a dimensionless number. In this way, the extent of variability in relation to the mean of the population can be taken into account. High CoV values could be related to high dispersion of data associable with coalescence transition stage. Vice versa, low CoV values can be related to more stable stage (e.g. completed or inhibited coalescence). Furthermore, the circularity, C, is defined as:

$$C = 4\pi \times \frac{(Area)}{(Perimeter)^2} \tag{4}$$

For a perfect circle, its value is 1.0. As the bubble shape is elongated or not regular, the circularity value tends to 0.0.

Table 1 shows that increasing salt hydrate content a reduction of average diameter of bubbles and of bubble areas occurred, indicating that silicone foaming is progressively hindered at greater filler content in the composite foam. At about 40-50% of salt hydrate a transition from lightweight-foamed structure to more dense structure takes place. This consideration is confirmed analysing the CoV trend at increasing filler content. Low CoV values were observed at low and high salt hydrate amount in the composite foam formulation. The maximum CoV value was observed for Mg_50

sample. This behaviour can be justified considering that at low filler content the coalescence is a main driving mechanism for bubble growth. The large coalescence phenomenon, occurring during the foaming stage, achieves the formation of a homogeneous distribution of large bubbles.

Conversely, at high filler content the coalescence phenomenon is drastically reduced and thus a homogeneous distribution of small bubbles is induced. A medium content of salt hydrate in the composite foam formulation (Mg_50) is characterised by a broad dispersion of bubble size (as confirmed by large CoV) due to limited coalescence activation.

Further information can be acquired analysing *Figure 4*~~Figure 4~~ where the circularity versus diameter distribution is reported for three reference silicone foams (Mg_0, Mg_40 and Mg_70 foams).

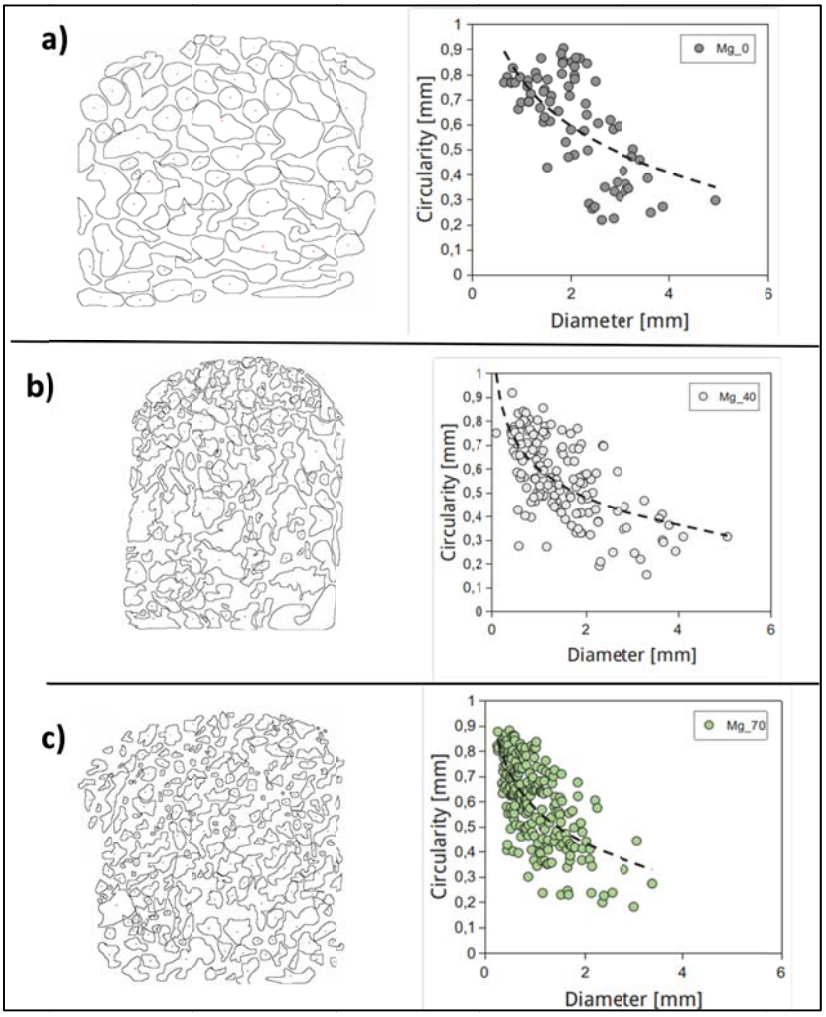

Figure 4: Boundary bubble distribution (left) and circularity evolution (right) at varying diameter for three reference composite foams filled with different salt amount. a) pure foam; b) Mg_40; c) Mg_70

Pure silicone foam (*Figure 4*~~Figure 5~~a) is characterised by large bubbles (average diameter size 2.12 mm). Most of the bubbles have a quite circular shape (circularity index >0.6) and an average cell size diameter of about 1.5 mm. Only few bubbles present a low circularity and large diameter (3-5 mm). The large diameter dimension observed in foam bubbles in Mg_0 sample is due to coalescence phenomena. Furthermore, the low viscosity of the composite slurry during the foam preparation stimulate the

formation of circular shaped bubbles. A progressive reduction of circularity at increasing bubble dimension is observed. This trend is a consequence of the interconnection between some bubbles during the foaming stage. The aggregation of these bubble domains, generated by coalesced bubbles, stimulates the presence of very large bubbles with low circularity [30]. However, an inversely proportional relationship between bubble size and circularity is confirmed. Indeed, all the composite foams have shown in their data distribution large dimensions in correspondence of low circularity of the bubbles (

Figure 4~~Figure 5~~b-c).

Although in Mg_70 foam sample (

Figure 4~~Figure 5~~c) a large amount of bubbles is identified by high circularity (circularity index in the range 0.6-0.9) and small cell size diameter (about 0.5mm), also bubbles with a circularity index lower than 0.3 have been found. These bubbles are characterised by a diameter of about 3 mm. This confirms the previous considerations concerning the difficulties of coalescence in foams with large amount of salt hydrate.

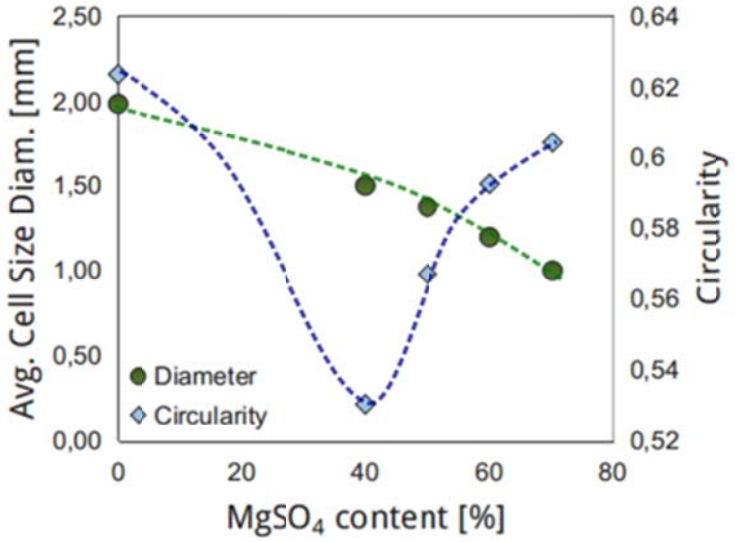

Figure 5: Average cell size diameter and circularity at increasing zeolite content

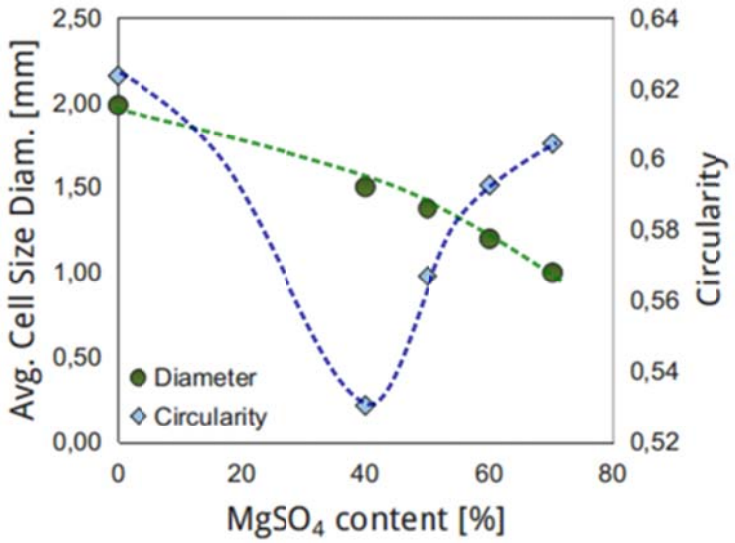

Figure 5~~Figure 6~~ summarizes the above cited considerations. The average foam diameter progressively decreases at increasing the salt hydrate content. A reduction of 25% of cell size diameter was observed with the addition of only 40% of filler in the silicone foam (from 2.12 to 1.70 for Mg_0 and Mg_40, respectively). This trend is confirmed also at higher filler content. In particular, a reduction of 50% of bubble size, compared to pure foam, can be observed in Mg_70 sample. The foam begins to become dense and more compact, due to the greater difficulty of foaming and the coalescence of the nascent bubbles, although there is still a significant and evident macro-porosity, which makes the Mg_70 composite foam potentially active for hydration/dehydration cycles.

Concerning the circularity index trend, it is clearly identified that a minimum happens at filler content of 40%. It can be justified considering that at low and medium content of salt hydrate, not all the generated bubbles have the possibility to complete the coalescence process. Consistently, when the siloxane matrix has terminated the condensation process, interconnected structures with complex geometry and low circularity remain to form the reticulated foam structure. This affects the distribution of the circularity of the bubbles, resulting in a lower average circularity index. On the contrary, in high salt content foams, almost all the bubbles have coalescence constraints due to the high viscosity of the formulation. As a result, small cell sizes with circular-shaped bubbles were observed. Differently for the unfilled foams, a very large quantity of generated bubbles complete the coalescence phase and therefore predominantly large circular-shaped cells were obtained. These consideration are summarised in *Figure 6*~~figure 7~~.

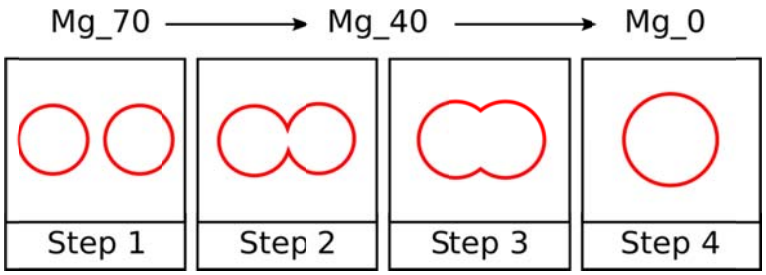

Figure 6: Scheme of bubble coalescence at increasing filler content highlights a skewed distribution for all the samples

Analysing the distribution modification at varying salt content some considerations can be extrapolated

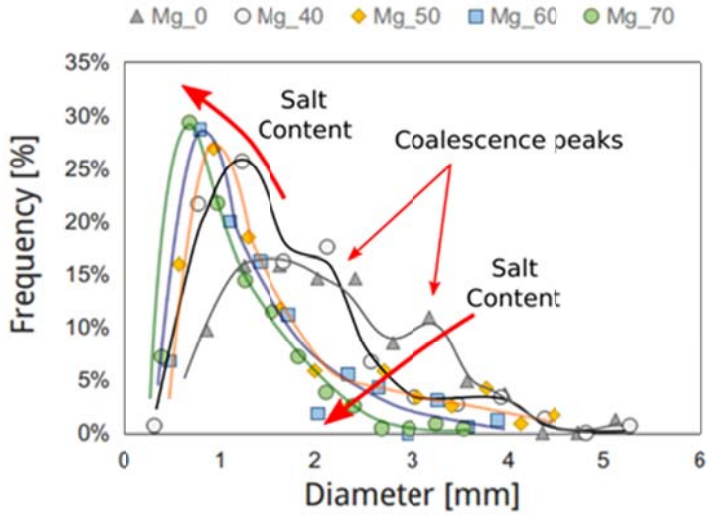

Figure 7~~Figure 8~~). The distribution frequency of diameter size of samples with low salt content is characterized by a low and wide multi-peak shape. Vice versa, with high salt content, the distribution tends to become increasingly high and narrow, with a skewness effect more and more concentrated at lower diameters.

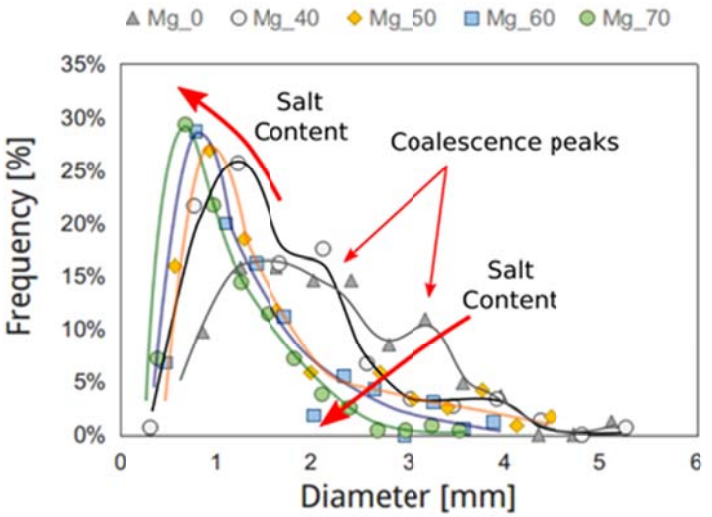

Figure 7: Frequency plot of diameter distribution for all composite foams

An evident effect is the shift of maximum frequency towards lower diameter, combined with the reduction of frequency counts observed in the diameter size range 2-4 mm. This aspect is related to the progressive reduction of coalescence phenomena for composite foams at higher salt content. In fact, the peak in frequency distribution observed at medium diameter size in Mg_0 and Mg_40 sample (highlighted in the plot as coalescence peaks) decrease progressively up to disappear~~s~~ for Mg_70 samples, where coalescence phenomena is heavily limited.

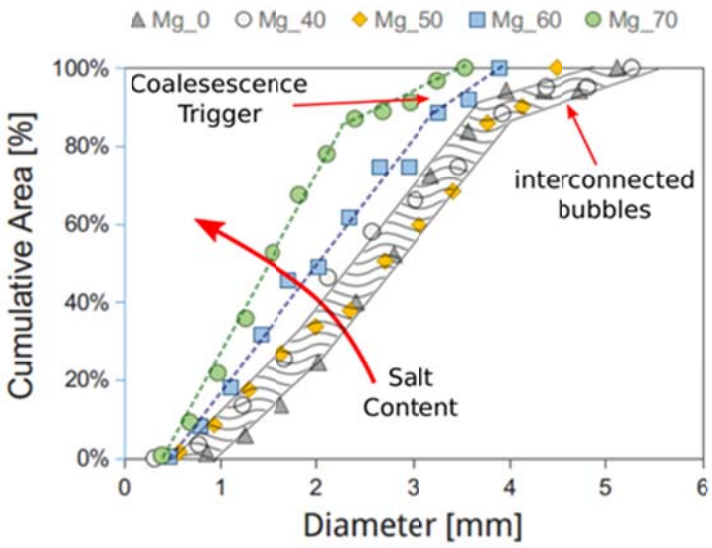

Figure 8: Cumulative area evolution at varying diameter for all composite foams

Figure ***8***~~Figure 9~~ shows the cumulative area percentage evolution at varying diameter for all composite foams. At increasing salt content, a progressive translation of curves toward smaller diameters is evidenced.

Unfilled and low salt content foams (Mg_40 and Mg_50) showed a quite similar trend. For these samples, the cumulative area curve starts larger cell size dimension than Mg_60 and Mg_70. The trend is characterised by three linear sections. The first section is mainly related to small size bubbles not coalesced. Its incidence reaches about 25% of cumulative area beyond which a knee in the trend of the curve is identifiable. Afterwards, the region with cumulative area in the 25% -80% range is associated with bubble size about 2-4 mm. As discussed above, this stage can be associated with the initiation and evolution of coalescence phenomena. Finally, the last portion of the curve, at cumulative area greater than 80%, is due to large bubbles (cell size >4mm). In this region, a strong inflection of the curve is evident. This was made possible by the formation of an interconnected local structure generated because of the coalescence of aggregate bubble domains. Further useful information can be drawn by analysing the trend of the cumulative area for Mg_70. The curve shows a linear trend up to a diameter of about 2 mm. The slope variation found at large cell size could be due to the initiation of coalescence phenomena, which although still at the embryonic level due to the high viscosity of the composite slurry, has been triggered resulting in an increase in the size of a contained portion of bubbles (anyway, this region affects only 15% of the cumulative area trend). It is worth stating that the presence of smaller bubbles homogeneously dispersed allows reducing the possibility to encounter coalesced salt crystals, that present a potential site where deliquescence can occur. Moreover, this should also increase the mechanical properties of the composite, which is then suitable for foaming in larger sizes (e.g. in flat-tube heat exchangers commonly used in thermochemical storages).

The performed analysis on the effect of salt content on the achievable porous structure of the composite foam allowed identifying critical conditions that cause transition from a foam configuration to another. These outcomes, coupled to the evaluation of hydration/dehydration behaviour, can give a better understanding about the most effective solution for the optimisation of these composite sorbents.

Hydration/Dehydration performances

The experimental analysis of hydration/dehydration performance was carried out by means of a thermo-gravimetric apparatus [31]~~[23]~~, able to work under saturated water vapour atmosphere. Particularly, dehydration tests were performed on synthesized samples as well as on the pure salt hydrate, keeping the water vapour pressure at 23.4 mbar and performing a heating ramp from 30°C up to 150°C. The analysis of the achieved results is summarised in Table 2. The actual salt content was obtained considering the difference between the dehydrated water content of the composite foam (normalized respect to filler content) and the pure salt. As evidenced in [28], the silicone foam does not influence the sorption properties of adsorbent filler, preserving its adsorption capability.

Table 2: Comparison between nominal and actual salt content for each sample, after experimental characterisation under real operating conditions

Sample	Nominal salt content [wt.%]	Actual salt content [wt.%]
Pure $MgSO_4 \cdot 7H_2O$	100	100
Mg_40	40	37.15
Mg_50	50	41.08
Mg_60	60	56.74
Mg_70	70	58.37

As reported in [27]~~[23]~~, discrepancy between nominal and actual salt content, between 3% and 12% for Mg_40 and Mg_70, respectively, has been evaluated. These differences can be related both to experimental issues during the composites preparations (e.g. partial dissolution of the salt, loss of salt during samples handling) as well as to hindering effect of the matrix against the hydration/dehydration reaction of the embedded salt. In the following paragraph, simplified schemes of possible mechanisms of water vapour diffusion inside the foam samples are presented, taking into account the analysis of the characterisations reported above.

Water vapour diffusion mechanism

Based on the information acquired from calorimetric tests and morphological analysis, a scheme of the possible vapour flow mechanism that could take place in the composite foams has been proposed. Indeed, this aspect is of the uttermost importance when considering the application in thermochemical storage systems, since it affects both the dynamics and the stability of the system. Two composite foams with different salt filler contents are compared. A low content salt hydrate foam is characterized by medium/large bubbles due to their coalescence during the foaming phase. Moreover, it has been hypothesized that some bubbles are partially interconnected, characterised by a complex geometry with a low circularity. Vice versa, the size of the bubbles in the composite foam with a high content of salt hydrate, is much lower. Moreover, this foam shows a lower foaming ratio and the bubbles do not undergo coalescence and are mainly not interconnected. A scheme of these morphologies is reported in *Figure 9*.

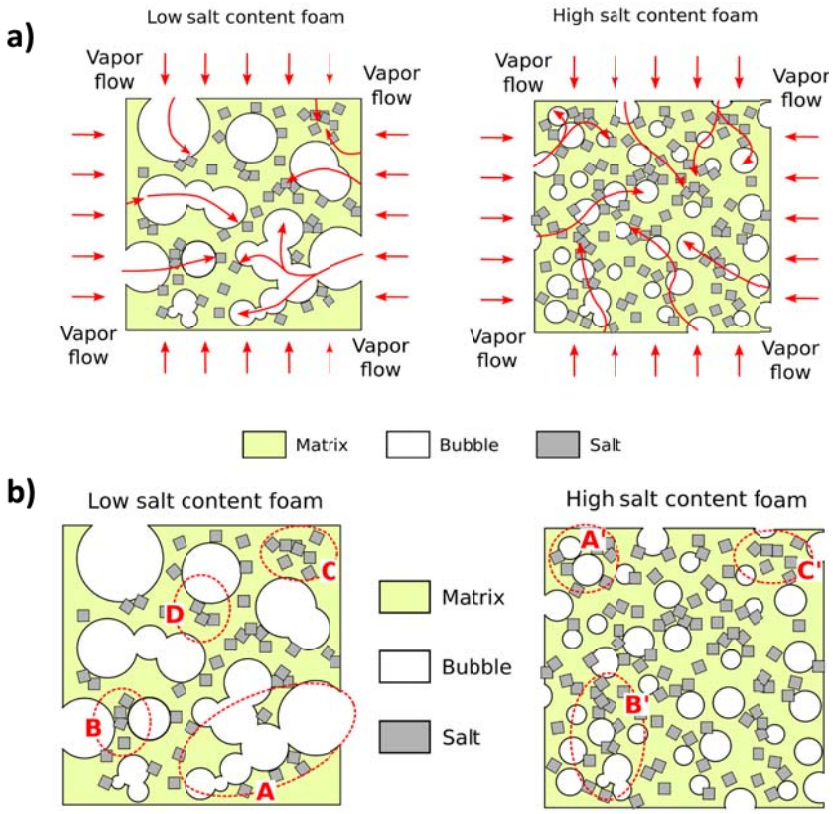

Figure 9: Scheme of foam morphology and vapour flow pathways in low salt (left) and high salt (right) composite foams

With low salt content, the vapour diffusion through the foam is ensured by the macro-porous structure of the cell foam (*Figure 9*~~Figure 10~~a). The water vapour flow is guaranteed at first by the cellular interconnection of the bubbles (point A in *Figure 9*~~Figure 10~~b) that represents a preferential flow pathway. Moreover, in consideration of the low thickness of the cell walls, also neighbouring bubbles can effectively contribute to a rapid vapour flow (point B *Figure 9*~~Figure 10~~b). In this area, the salt hydrate embedded in the silicon matrix can easily interact with the vapour phase, facilitating its hydration/dehydration. The salt hydration/dehydration can be also allowed by secondary flow

lines (point D in *Figure 9*~~Figure 10~~b) induced by salt hydrate domains just in proximity of bubble border.

Not all of the salt hydrate is able to provide a rapid hydration/dehydration process. The crystals of salt, shielded by thick siloxane matrix layer, could be inactive (point C in *Figure 9*~~Figure 10~~b). However, considering the high vapour permeability of the PDMS, a possible energy storage contribution, although kinetically limited by diffusion aspects, can also be provided by these salt hydrate areas.

High salt hydrate filled composite foam is characterised by a quite different cellular structure. Bubbles have a small diameter size. Furthermore, the cell wall becomes thick considering that the distance among bubbles become larger. Occasionally, some contiguous bubbles can be observed (point A' in *Figure 9*~~Figure 1~~0b), ensuring a preferential water vapour flow through the contiguous boundary *Figure 9*~~Figure 10~~a).

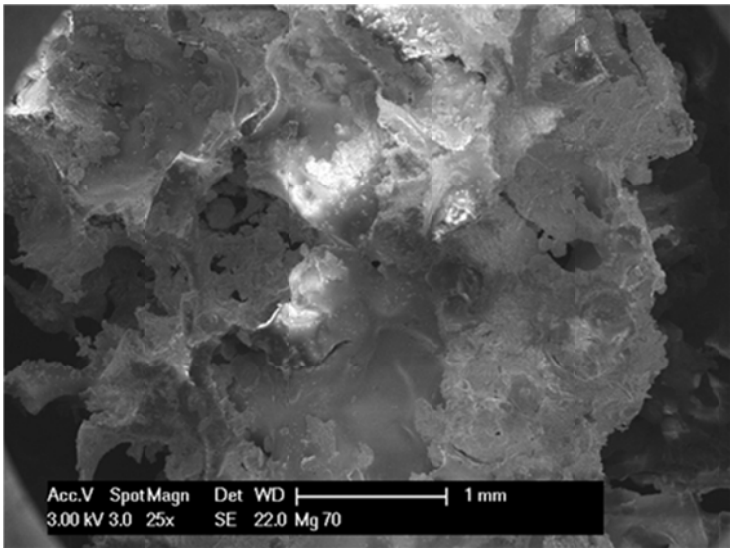

Figure 10: SEM image at 25x magnification of Mg_70 foam.

In order to validate the hypothesized structure of the foam composite at high salt hydrate content and to better highlight the ~~the~~ framework microstructural homogeneity of the foam the SEM image at high magnification of a Mg_70 sample was taken in *Figure* ***10***~~Figure 11~~. The silicone matrix appears compact and homogeneous. Some small micro-cracks can be also identified. Furthermore, some salt hydrate domains can be observed in the cellular structure of the composite foam.

The formation of these areas of long-range connectivity, due to a random contiguous distribution of the salt grains in the bulk of the silicone matrix, allows the activation of further preferential paths for the water vapour flow (point B' in the *Figure 9*~~Figure 10~~b). In this way, a larger amount of salt is involved in the hydration/dehydration process and a more homogeneous behaviour of the different parts of the composite is ensured. This is especially important when considering the realisation of

full-scale components, where inhomogeneity in foam morphology or reaction behaviour at different thicknesses and heights can limit the overall storage capacity.

Therefore, a large amount of the salt filler is able to guarantee its hydration/dehydration capabilities by principal or secondary flow channels, giving large potential applicability of these composite foams. Only some rare salt grains are insulated in the siloxane matrix limiting its interaction with water vapour (point C' in *Figure 9*~~Figure 10~~b). However, for high salt content foam the probability to find insulated filler grains embedded in thick siloxane matrix is heavily reduced

Conclusion

An innovative MgSO4·7H20 silicone composite foam was developed for sorption thermal energy storage applications. In particular, in this work, morphological aspects on sorption performance of the salt-silicone foam at varying filler content (40-70 wt.% salt content) were investigated. By morphological investigation it was evidenced that the foam is constituted by a mixed open/closed pore structure. At increasing filler content, a gradual reduction in open porosity and bubble size was found. However, the reduced foaming ratio for specimens with higher salt content did not influence de/hydration capabilities of the foam. The thermo-physical tests, carried out for all the composite foams, showed good dehydration performance, indicating that the silicon matrix does not hinder the diffusion of water vapour. Based on de/hydration capability and morphological analysis a simplified scheme of water vapour diffusion process was proposed for both low and high salt content composite foam.

Acknowledgements

The present work was partially funded by PON “Ricerca e Competitività 2007-13” PON03PE_00206_2 S5 - Smart Small Scale Solar Systems. The work was partially funded by the Spanish government (ENE2015-64117-C5-1-R). The authors would like to thank the Catalan Government for the quality accreditation given to her research group (2017 SGR 1537). GREA is certified agent TECNIO in the category of technology developers from the Government of Catalonia.

References

[1] N.L. Le, S.P. Nunes, Materials and membrane technologies for water and energy sustainability, Sustain. Mater. Technol. (2016). doi:10.1016/j.susmat.2016.02.001.

[2] A. Ivancic, D. Mugnier, G. Stryi-Hipp, W. Weiss, Solar Heating and Cooling Technology Roadmap, 2014. doi:10.1007/SpringerReference_7300.

[3] L. Miró, J. Gasia, L.F. Cabeza, Thermal energy storage (TES) for industrial waste heat (IWH) recovery: A review, Appl. Energy. (2016). doi:10.1016/j.apenergy.2016.06.147.

[4] G. Alva, Y. Lin, G. Fang, An overview of thermal energy storage systems, Energy. (2018). doi:10.1016/j.energy.2017.12.037.

[5] J. Lizana, R. Chacartegui, A. Barrios-Padura, J.M. Valverde, Advances in thermal energy storage materials and their applications towards zero energy buildings: A critical review, Appl. Energy. (2017). doi:10.1016/j.apenergy.2017.06.008.

[6] A. Gutierrez, S. Ushak, V. Mamani, P. Vargas, C. Barreneche, L.F. Cabeza, M. Grágeda, Characterization of wastes based on inorganic double salt hydrates as potential thermal energy storage materials, Sol. Energy Mater. Sol. Cells. (2017). doi:10.1016/j.solmat.2017.05.036.

[7] M. Gaeini, A.L. Rouws, J.W.O. Salari, H.A. Zondag, C.C.M. Rindt, Characterization of microencapsulated and impregnated porous host materials based on calcium chloride for thermochemical energy storage, Appl. Energy. (2018). doi:10.1016/j.apenergy.2017.12.131.

[8] M. Richter, E.M. Habermann, E. Siebecke, M. Linder, A systematic screening of salt hydrates as materials for a thermochemical heat transformer, Thermochim. Acta. (2018). doi:10.1016/j.tca.2017.06.011.

[9] N. Yu, R.Z.Z. Wang, L.W.W. Wang, Sorption thermal storage for solar energy, Prog. Energy Combust. Sci. 39 (2013) 489–514. doi:10.1016/j.pecs.2013.05.004 Review.

[10] G. Krese, R. Koželj, V. Butala, U. Stritih, Thermochemical seasonal solar energy storage for heating and cooling of buildings, Energy Build. (2018). doi:10.1016/j.enbuild.2017.12.057.

[11] L.F. Cabeza, A. Solï¿½, C. Barreneche, Review on sorption materials and technologies for heat pumps and thermal energy storage, Renew. Energy. (2017). doi:10.1016/j.renene.2016.09.059.

[12] A. Frazzica, A. Freni, Adsorbent working pairs for solar thermal energy storage in buildings, Renew. Energy. (2017). doi:10.1016/j.renene.2016.09.047.

[13] G. Santori, C. Di Santis, Optimal fluids for adsorptive cooling and heating, Sustain. Mater. Technol. (2017). doi:10.1016/j.susmat.2017.04.005.

[14] P.A.J. Donkers, L.C. Sögütoglu, H.P. Huinink, H.R. Fischer, O.C.G. Adan, A review of salt hydrates for seasonal heat storage in domestic applications, Appl. Energy. (2017).

doi:10.1016/j.apenergy.2017.04.080.

[15] D. Alby, F. Salles, J. Fullenwarth, J. Zajac, On the use of metal cation-exchanged zeolites in sorption thermochemical storage: Some practical aspects in reference to the mechanism of water vapor adsorption, Sol. Energy Mater. Sol. Cells. (2018). doi:10.1016/j.solmat.2017.11.020.

[16] S.K. Henninger, F.P. Schmidt, H.M. Henning, Characterisation and improvement of sorption materials with molecular modeling for the use in heat transformation applications, in: Adsorption, 2011. doi:10.1007/s10450-011-9342-6.

[17] F.K. Martijn F. de Lange, Karlijn J. F. M. Verouden, Thijs J. H. Vlugt, Jorge Gascon, Adsorption-Driven Heat Pumps: The Potential of Metal–Organic Frameworks, Chem. Rev. 115 (2015) 12205–12205. doi:10.1021/acs.chemrev.5b00059.

[18] E.A. Levitskij, Y.I. Aristov, M.M. Tokarev, V.N. Parmon, “Chemical Heat Accumulators”: A new approach to accumulating low potential heat, Sol. Energy Mater. Sol. Cells. (1996). doi:10.1016/0927-0248(96)00010-4.

[19] L.G. Gordeeva, Y.I. Aristov, Composites “salt inside porous matrix” for adsorption heat transformation: A current state-of-the-art and new trends, Int. J. Low-Carbon Technol. (2012). doi:10.1093/ijlct/cts050.

[20] E. Courbon, P. D’Ans, A. Permyakova, O. Skrylnyk, N. Steunou, M. Degrez, M. Frère, A new composite sorbent based on SrBr2 and silica gel for solar energy storage application with high energy storage density and stability, Appl. Energy. (2017). doi:10.1016/J.APENERGY.2017.01.041.

[21] Y.N. Zhang, R.Z. Wang, Y.J. Zhao, T.X. Li, S.B. Riffat, N.M. Wajid, Development and thermochemical characterizations of vermiculite/SrBr2 composite sorbents for low-temperature heat storage, Energy. 115 (2016) 120–128. doi:10.1016/J.ENERGY.2016.08.108.

[22] A.D. Grekova, L.G. Gordeeva, Y.I. Aristov, Composite “LiCl/vermiculite” as advanced water sorbent for thermal energy storage, Appl. Therm. Eng. 124 (2017) 1401–1408. doi:10.1016/J.APPLTHERMALENG.2017.06.122.

[23] S. Hongois, F. Kuznik, P. Stevens, J.J. Roux, Development and characterisation of a new MgSO4-zeolite composite for long-term thermal energy storage, Sol. Energy Mater. Sol. Cells. (2011). doi:10.1016/j.solmat.2011.01.050.

[24] M. Tokarev, L. Gordeeva, V. Romannikov, I. Glaznev, Y. Aristov, New composite sorbent CaCl2 in mesopores for sorption cooling/heating, Int. J. Therm. Sci. 41 (2002) 470–474. doi:10.1016/S1290-0729(02)01339-X.

[25] J.Y. Wang, R.Z. Wang, L.W. Wang, Water vapor sorption performance of ACF-CaCl2 and silica gel-CaCl2 composite adsorbents, Appl. Therm. Eng. 100 (2016) 893–901.

doi:10.1016/J.APPLTHERMALENG.2016.02.100.

[26] A. Jabbari-Hichri, S. Bennici, A. Auroux, CaCl2-containing composites as thermochemical heat storage materials, Sol. Energy Mater. Sol. Cells. 172 (2017) 177–185. doi:10.1016/J.SOLMAT.2017.07.037.

[27] V. Palomba, A. Solé, L. Calabrese, V. Brancato, Experimental characterization of composite materials for thermochemical energy storage with foam matrices, in: 14th Int. Conf. Energy Storage, Adana, Turkey, 2018.

[28] L. Calabrese, L. Bonaccorsi, A. Freni, E. Proverbio, Synthesis of SAPO-34 zeolite filled macrocellular foams for adsorption heat pump applications: A preliminary study, Appl. Therm. Eng. (2017). doi:10.1016/j.applthermaleng.2017.06.121.

[29] L. Calabrese, L. Bonaccorsi, A. Freni, E. Proverbio, Silicone composite foams for adsorption heat pump applications, Sustain. Mater. Technol. (2017). doi:10.1016/j.susmat.2017.04.002.

[30] L. Calabrese, L. Bonaccorsi, P. Bruzzaniti, A. Freni, E. Proverbio, Morphological and functional aspects of zeolite filled siloxane composite foams, J. Appl. Polym. Sci. 135 (n.d.) 45683. doi:10.1002/app.45683.

[31] A. Frazzica, A. Sapienza, A. Freni, Novel experimental methodology for the characterization of thermodynamic performance of advanced working pairs for adsorptive heat transformers, Appl. Therm. Eng. 72 (2014) 229–236. doi:10.1016/J.APPLTHERMALENG.2014.07.005.

[32] A.K.S. Chesterton, D.A.P. De Abreu, G.D. Moggridge, P.A. Sadd, D.I. Wilson, Evolution of cake batter bubble structure and rheology during planetary mixing, Food Bioprod. Process. (2013). doi:10.1016/j.fbp.2012.09.005.

[33] H.A. Sturges, The Choice of a Class Interval, J. Am. Stat. Assoc. (1926). doi:10.1080/01621459.1926.10502161.